

# Tempora: Characterising the Time-Contingent Utility of Online Test-Time Adaptation

Sudarshan Sreeram<sup>1</sup> Young D. Kwon<sup>2</sup> Cecilia Mascolo<sup>1</sup>

## Abstract

Test-time adaptation (TTA) offers a compelling remedy for machine learning (ML) models that degrade under domain shifts, improving generalisation *on-the-fly* with only unlabelled samples. This flexibility suits real deployments, yet conventional evaluations unrealistically assume unbounded processing time, overlooking the accuracy-latency trade-off. As ML increasingly underpins latency-sensitive and user-facing use-cases, temporal pressure constrains the viability of adaptable inference; predictions arriving too late to act on are futile. We introduce *Tempora*, a framework for evaluating TTA under this pressure. It consists of temporal scenarios that model deployment constraints, evaluation protocols that operationalise measurement, and time-contingent utility metrics that quantify the accuracy-latency trade-off. We instantiate the framework with three such metrics: **1** *discrete* utility for asynchronous streams with hard deadlines, **2** *continuous* utility for interactive settings where value decays with latency, and **3** *amortised* utility for budget-constrained deployments. Applying Tempora to seven TTA methods on ImageNet-C across 240 temporal evaluations reveals *rank instability*: conventional rankings do not predict rankings under temporal pressure; ETA, a state-of-the-art method in the conventional setting, falls short in 41.2% of evaluations. The highest-utility method varies with corruption type and temporal pressure, with no clear winner. By enabling systematic evaluation across diverse temporal constraints for the first time, Tempora reveals when and why rankings invert, offering practitioners a lens for method selection and researchers a target for deployable adaptation.

<sup>1</sup>Department of Computer Science and Technology, University of Cambridge, Cambridge, England, United Kingdom <sup>2</sup>Samsung AI Center, Cambridge, England, United Kingdom. Correspondence to: Sudarshan Sreeram <ss3122@cam.ac.uk>.

Preprint. February 9, 2026.

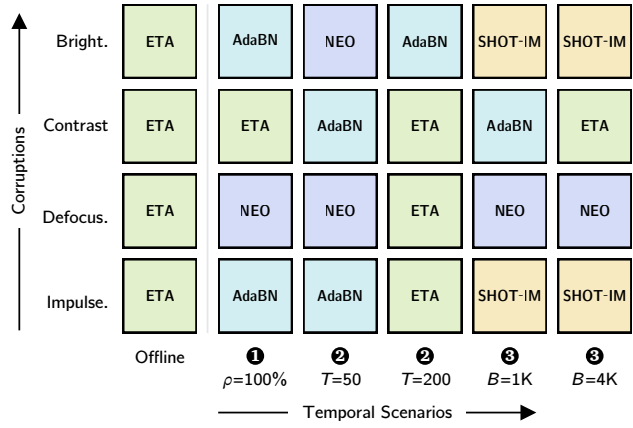


**Figure 1. Rank instability across temporal evaluations.** Cells show the highest-utility method among seven TTA methods tested on ImageNet-C (ResNet-50). *Offline*: No time constraints. *Temporal*: **1** Discrete (hard deadlines), **2** Continuous (latency penalties), and **3** Amortised (budgeted overhead); formal definitions in §3. Rows reveal *rank instability*: the best method changes under temporal pressure. Similarly, columns show no consistent winner within any scenario. Aggregate benchmarks obscure these corruption-level dynamics. Extended results appear in Appendix C.

## 1. Introduction

Machine learning models increasingly serve as essential components of non-stationary real-world systems, from on-device scene analysis in computational photography (Apple, 2022) to tumour segmentation in clinical decision support (Dorfner et al., 2025). Standard inference treats these models as static artefacts and assumes that representations learned on fixed training distributions can inherently generalise to settings where the test distribution  $\mathcal{T}$  drifts stochastically. However, this assumption is fragile: a ResNet-50 model (He et al., 2016) achieving 76.1% accuracy on ImageNet (Russakovsky et al., 2015) drops to 18% on ImageNet-C corruptions (Niu et al., 2022; Hendrycks & Dietterich, 2019); in practice, such corruptions arise unpredictably in systems like wildlife camera traps, where species classifiers face site-specific conditions unseen during training.

Test-time adaptation (TTA) addresses this fragility by treating inference as an adaptive process rather than a static endpoint. In the “*Fully TTA*” setting (Wang et al., 2021),

in-situ calibration uses only the incoming stream  $x_i \sim \mathcal{T}$  and pre-trained parameters  $\theta$  to bridge the generalisation gap, not requiring training data, labels, or server-side infrastructure. This flexibility becomes essential as models scale. Training-time robustness via augmentation cannot feasibly cover the combinatorial space of real-world shifts (Sun et al., 2020)<sup>1</sup>, and model economics increasingly favour reuse over per-scenario re-training (Bommasani et al., 2021). While TTA enables this reuse, it is not without cost. Unlike standard inference, TTA introduces overhead, whether through closed-form solutions, gradient updates, or iterative optimisation. These costs lie on the critical path of each prediction, making a system’s response time a function of design choices that current evaluation methodology ignores.

Crucially, these evaluations typically assume unbounded processing overhead for adaptation, releasing a new batch only after adaptation on the previous batch completes; we term this *offline*. However, in latency-sensitive deployments, a correct prediction arriving after a user has closed an app or a robot has committed to an action is futile; correctness and timeliness are jointly necessary. Latency, when reported, appears only to substantiate aggregate efficiency gains rather than to serve as a constraint that determines system viability.

Alfarra et al. (2024) surfaced this tension by using a method’s processing overhead to limit adaptation opportunities; slower methods receive fewer batches. Their evaluation addresses a *discrete* temporal scenario where missing a deadline yields no value. However, real-world deployments span at least two more scenarios. First, in interactive systems, late predictions degrade user experience rather than causing outright failure; an on-device photo organiser that auto-tags images during bulk upload remains useful with a brief delay, but users grow impatient with longer waits. Second, some systems constrain total adaptation overhead while remaining agnostic to per-prediction latency. A drone performing visual crop inspection may budget onboard compute to preserve battery, requiring only that the mission completes before power runs out.

Without systematic coverage of these scenarios, practitioners cannot identify which methods fit their temporal constraints, and researchers lack a target for designing methods that will. Genuinely deployable methods justify their overhead through accuracy gains, integrating naturally into latency-sensitive systems; *computationally insolvent* methods consume budgets no accuracy benefit can repay. As methods grow increasingly sophisticated, temporal evaluation becomes essential; without it, the field risks chasing offline accuracy while producing methods that cannot serve real-world systems where adaptation is most needed.

<sup>1</sup>While safety-critical systems may pre-train on anticipated shifts, exhaustive coverage of real-world conditions is infeasible. TTA targets the residual shifts that escape such anticipation.

In this paper, we introduce *Tempora*, a framework for evaluating TTA under temporal constraints. It comprises temporal scenarios (contextualising deployments), evaluation protocols (operationalising measurement), and time-contingent utility metrics (quantifying the accuracy-latency trade-off). We instantiate this framework with three metrics for distinct scenarios (§3): ① *Discrete utility* for hard deadlines, ② *Continuous utility* for interactive responses, and ③ *Amortised utility* for budget-constrained deployments. Each couples accuracy with a scenario-appropriate temporal penalty; together, they map utility across the deployment space rather than a single point in a temporal vacuum.

**Contributions.** We reveal three findings by evaluating seven well-known Fully TTA methods across 16 temporal scenarios on the 15 shifts of ImageNet-C with ResNet-50<sup>2</sup>:

- *Rank instability.* The method deemed optimal under offline evaluation frequently underperforms under temporal pressure (Fig. 1). Of 240 temporal evaluations, the clear offline winner, ETA (Niu et al., 2023), loses in 99 cases (41.2%) and yields 19.3% utility on average to the winner. Practitioners and researchers cannot select a TTA method based solely on offline accuracy, yet current state-of-the-art method papers report only this (Murphy et al., 2025; Niu et al., 2025); evaluation must also occur under temporal scenarios.
- *Corruption-specific trade-offs.* Rank instability varies with corruption type: under continuous evaluation with a 50 ms response window, Spearman correlation with the offline ranking ranges from  $r_s = -0.74$  (brightness) to  $r_s = 0.21$  (Gaussian noise); negative values imply that offline ranking misleads method selection. The variation arises as corruptions perturb features differently, yet methods allocate compute uniformly. Deployable adaptation requires corruption-conditioned compute allocation: brightness shifts all pixels uniformly and corrects cheaply, while Gaussian noise perturbs pixels independently, requiring more compute to recover structure. However, estimating corruption difficulty without supervision remains an open question.
- *Pressure-specific trade-offs.* Rank instability increases with temporal pressure: under amortised evaluation, SHOT-IM (Liang et al., 2020) dominates at tight budgets, while ETA (Niu et al., 2022) dominates when budgets relax; correlation with the offline ranking jumps from  $r_s = 0.32$  to  $r_s = 0.96$  across this transition. This pattern holds across scenarios, with no single method dominating across pressure levels. Methods differ in their return on compute, and without knowing

<sup>2</sup>We use this conventional, episodic TTA benchmark to enable direct comparison with prior works. However, Tempora extends readily to other architectures and datasets.

operating conditions in advance, deployable adaptation requires time-aware scaling to meet temporal constraints and anytime properties: if a device suspends adaptation early to preserve battery, the elapsed compute should have yielded gains over standard inference.

While conventional evaluation of TTA methods asks which is most accurate, Tempora reframes evaluation to ask which delivers acceptable accuracy at a viable cost. This revised framing informs both method selection and design. For selection, rank instability under temporal pressure reveals winners that offline rankings obscure. For design, utility decompositions expose not just which methods win but why others fail, whether due to missed batches, slow responses, or unproductive overhead. With this lens, adaptation can, for the first time, be systematically evaluated across the temporal constraints of real-world systems it aims to serve.

## 2. Background & Related Work

**Domain Shifts.** Models trained on a source distribution  $\mathcal{S}$  often degrade when deployed on a target distribution  $\mathcal{T}$  where  $\mathcal{S} \neq \mathcal{T}$ . The degradation depends on what changes between the distributions. This paper focuses on covariate shift, which occurs when the input marginals differ, *i.e.*,  $\mathcal{P}_{\mathcal{S}}(\mathbf{X}) \neq \mathcal{P}_{\mathcal{T}}(\mathbf{X})$ , whilst the conditional  $\mathcal{P}(\mathbf{Y}|\mathbf{X})$  remains stable (Sugiyama et al., 2007). For example, wildfires cast an unnatural orange haze, causing the appearance of *known* objects to differ. While other shifts exist, TTA literature predominantly benchmarks against covariate shifts induced by *corruptions* (Hendrycks & Dietterich, 2019).

**Test-Time Adaptation.** Approaches to handling these shifts vary by data availability and temporal scope. We focus on *Fully Test-Time Adaptation* (Fully TTA) (Wang et al., 2021), which constrains adaptation to the test environment using only pre-trained parameters  $\theta$  and incoming unlabelled samples  $x_i \sim \mathcal{T}$ . This precludes access to source data or target labels, ensuring broad applicability as a drop-in enhancement for standard inference pipelines. We further focus on the *online* setting, which imposes a sequential commitment: the system must predict on the current input before observing the next input, necessitating *in-situ* processing.

**Adaptation Overhead.** Existing Fully TTA methods can be categorised by the component of the inference pipeline they modify, which informs their computational overhead. *Input adaptation* methods (Gao et al., 2023) project samples back to the source domain. *Output adaptation* (Boudiaf et al., 2022) and *activation adaptation* (Liu et al., 2021; Murphy et al., 2025) adjust logits or features directly, often keeping the backbone frozen. The most common category, *parameter adaptation* (Wang et al., 2021; Niu et al., 2022; Liang et al., 2020), updates network weights, typically affine parameters in normalisation layers, via backpropagation on

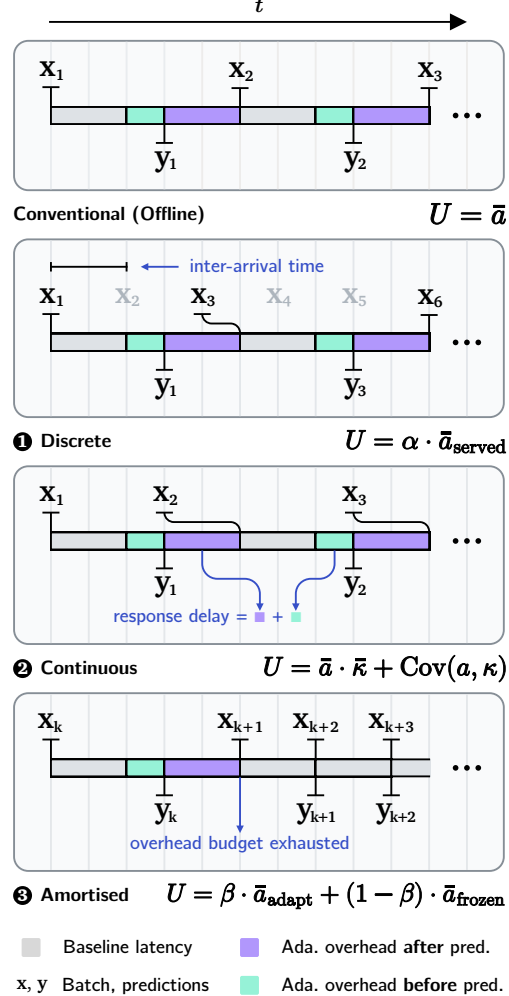


**Figure 2. Evaluation protocols for measuring time-contingent utility.** Each panel depicts the interaction between an input stream, a single model pipeline, and predictions over time  $t$ . Processing batch  $x_i$  to emit prediction  $y_i$  incurs baseline latency (grey), intrinsic overhead (green) that delays emission, and extrinsic overhead (purple) that stalls the pipeline before the next batch can begin; methods vary in their overhead profile. *Offline*: The stream waits for adaptation to complete before releasing the next batch; utility is the mean accuracy. **① Discrete**: Batches arrive asynchronously at fixed intervals; those arriving while the pipeline is occupied are skipped, so utility scales with availability  $\alpha$ . **② Continuous**: The stream releases  $x_{i+1}$  upon receiving  $y_i$  (greedy user); response delay incurs hyperbolic penalty  $\kappa$ . **③ Amortised**: Follows offline until overhead budget is exhausted, then frozen inference only; utility is a weighted combination over both phases.

self-supervised objectives such as entropy minimisation.

**Evaluation Contexts.** Conventional, offline evaluation ignores how this overhead interacts with accuracy, unrealistically assuming unbounded time to serve predictions; see Figure 2. Recent progress on improving evaluation has focused on *distributional* realism and *epistemic* practices. BoTTA (Danilowski et al., 2025) models scenarios with

limited data and non-stationary streams; UniTTA (Du et al., 2025) models 36 such streams via a Markov state-transition matrix. TTAB (Zhao et al., 2023b) evaluates beyond covariate shifts and also critiques hyperparameter sensitivity and pre-trained model selection. However, the *operational* context, specifically the temporal pressure imposed by the wider system, remains under-explored.

**Temporal Pressure.** Alfarra et al. (2024) address this gap by penalising slow adaptation with fewer batches from an asynchronous data stream. Batches arrive at intervals  $\gamma$  set to the standard inference latency, which corresponds to 100% pipeline utilisation. When the wall-clock time under adaptation  $\delta$  exceeds  $\gamma$ ,  $\lceil \delta/\gamma \rceil - 1$  subsequent batches bypass adaptation and receive predictions from a fallback model. While this formalises sample starvation as a penalty for overhead, the protocol presents three limitations:

- *Risk-free evaluation*: The fallback model guarantees valid predictions, masking cases where adaptation is unavailable. Also, it assumes zero-cost parallel model execution, which is often prohibitive in resource-scarce settings typical of edge deployments. We build on the more realistic single-model variant noted in Alfarra et al.’s (2024) appendix to compute discrete utility.
- *Disproportionate penalties*: The ceiling operation creates stepped penalties that obscure incremental efficiency gains. For  $\gamma = 100$  ms, any  $\delta \in (100, 200]$  ms incurs a 50% miss rate despite nearly 2 $\times$  variation in overhead. In general, any  $\delta \in (k\gamma, (k+1)\gamma]$  maps to the same miss rate  $1 - 1/(k+1)$ , and optimisations within a tier go unrewarded.
- *Forced idling*: The protocol enforces rigid synchronisation, where a batch arriving at  $t$  is treated as missed if adaptation is not ready exactly at  $t$ . Consequently, a method completing at  $t + \epsilon$  idles for nearly  $\gamma$  despite being available, wasting the window to serve batch  $t$ .

Given these limitations, the following section introduces Tempora, a framework for evaluating TTA under temporal constraints that models the accuracy-latency trade-off beyond just discrete temporal semantics. Further details on Alfarra et al.’s (2024) protocol appear in Appendix B.

### 3. Tempora

Conventional evaluations decouple theoretical accuracy from operational utility; they model inference as a static mapping  $f_\theta : \mathcal{X} \rightarrow \mathcal{Y}$ , reporting mean accuracy  $\bar{a} = \frac{1}{N} \sum \mathbb{1}(f_{\theta_i}(x_i) = \hat{y}_i)$  and implicitly assuming unbounded processing time. Although works report latency to supplement efficiency claims (Niu et al., 2022), it only captures static, aggregate speedups. This decoupling obscures the

temporal regimes in which methods remain viable; diffusion-based input adaptation (Gao et al., 2023), for instance, is 810 $\times$  slower than naive inference (Alfarra et al., 2024).

In this paper, we formalise the data stream as a sequence of tuples  $\{(\mathbf{x}_i, t_i)\}_{i=1}^N$ , where  $N$  is the total number of batches and  $t_i$  denotes the arrival time of batch  $\mathbf{x}_i$ . We then address the evaluation gap identified in §2 by introducing three time-contingent metrics that define operational utility  $U(\{(\mathbf{y}_i, \delta_i)\}_{i=1}^N)$  as a functional that maps the joint trajectory of predictions  $\mathbf{y}_i$  and latency  $\delta_i$  to a scalar value; this conditions utility on both correctness and timeliness. We structure these metrics around three archetypes: *discrete* (environment-led), *continuous* (user-led), and *amortised* (resource-led). The following sections formalise each archetype alongside its temporal scenario, evaluation protocol, and utility metric; together, they form *Tempora*. Concrete examples and parameter choices appear in §4.1.

#### 3.1. Discrete Utility

**Scenario.** Following Alfarra et al. (2024), we begin with the most constrained setting: asynchronous streams where batches arrive at fixed intervals despite the readiness of a single-model prediction pipeline. This models autonomous systems, sensor networks, and monitoring applications where data arrives at rates dictated by external processes. If the pipeline cannot keep pace, batches are lost irrecoverably.

**Protocol.** Batches arrive at times  $t_i = (i-1)\gamma$  for inter-arrival time  $\gamma > 0$ . When processing completes, the pipeline serves the most recent arrival; intervening batches are forfeit. We address the disproportionate penalties and forced idling limitations by introducing a batch-sized buffer that holds the incoming batch in memory from  $t_i$  to  $t_i + \gamma$ . Appendix B elaborates on our revision of Alfarra et al.’s (2024) protocol.

Let  $(s_j, f_j)$  denote the start and finish times of the  $j$ -th processing event, with  $s_1 = 0$  and  $f_1 = \delta_1$ . The recurrence  $s_{j+1} = \max(f_j, t_{p_{j+1}})$  and  $f_{j+1} = s_{j+1} + \delta_{p_{j+1}}$  governs timing, where  $p_j$  denotes the batch served at event  $j$ :  $p_1 = 1$  and  $p_{j+1} = \max(p_j + 1, \lfloor f_j/\gamma \rfloor + 1)$ . This captures two regimes: when  $\delta_i < \gamma$ , processing outpaces arrivals and  $p_j = j$ ; when  $\delta_i > \gamma$ , the pipeline falls behind and batches are skipped. Replacing +1 with +2 in the floor term recovers Alfarra et al.’s (2024) stricter synchronisation.

**Metric.** Let  $\mathcal{P}$  denote the set of served batch indices and  $a_i$  the accuracy on batch  $i$ . Discrete utility is formally:

$$U_{\text{discrete}} = \frac{1}{N} \sum_{i \in \mathcal{P}} a_i = \underbrace{\frac{|\mathcal{P}|}{N}}_{\alpha} \cdot \underbrace{\frac{1}{|\mathcal{P}|} \sum_{i \in \mathcal{P}} a_i}_{\bar{a}_{\text{served}}} \quad (1)$$

Availability  $\alpha = |\mathcal{P}|/N$ , the fraction of batches served, and served accuracy  $\bar{a}_{\text{served}}$  separate two failure modes: system errors and model errors. Given standard inference accuracy

$a_0$ , a method must achieve  $\bar{a}_{\text{served}} > a_0/\alpha$  to outperform standard inference; for  $\alpha = 0.5$ , accuracy must double, a requirement that most methods fail to meet.

### 3.2. Continuous Utility

**Scenario.** Discrete utility models environment-led arrivals, but not all systems impose rigid schedules. Timeliness is often governed by interactivity or downstream service-level constraints, where excess latency degrades user experience. We model this via a greedy user who submits batch  $i + 1$  upon receiving  $\mathbf{y}_i$ ; the stream synchronises with prediction emission, and no batches are skipped. This represents maximal demand on pipeline responsiveness.

**Protocol.** We penalise latency via hyperbolic decay (Mazur, 1987), consistent with evidence linking subjective time perception to value discounting (Brocas et al., 2018). This formulation captures non-linear user patience: a lag of 100 ms is perceptually sharper than an equivalent slip at 1 s.

Let  $\lambda$  denote standard inference latency. We decompose  $\delta_i = e_i + \ell_i$  at the prediction boundary, where  $e_i$  spans pickup to prediction and  $\ell_i$  spans prediction to availability. This reveals two types of adaptation overhead: *intrinsic* overhead  $e_i - \lambda$  delays the immediate response, while *extrinsic* overhead  $\ell_i$  stalls the pipeline before the next batch is picked up; see Figure 2. The user experiences wait time  $w_i = \ell_{i-1} + e_i$ , with  $\ell_0 = 0$ , resulting in an effective response delay  $d_i = \max(0, w_i - \lambda)$ .

**Metric.** Continuous utility is formally:

$$U_{\text{continuous}} = \frac{1}{N} \sum_{i=1}^N a_i \kappa_i = \bar{a} \cdot \bar{\kappa} + \text{Cov}(a, \kappa) \quad (2)$$

where  $\kappa_i = (1 + d_i/(T - \lambda))^{-1}$  is a decay factor that discounts accuracy using a human-computer interaction (HCI) threshold  $T > \lambda$ ; value halves when  $w_i = T$ , and a lower  $T$  imposes more temporal pressure. It accommodates service-level constraints where deadlines are targets, not cliffs. The decomposition of utility separates accuracy  $\bar{a}$  from responsiveness  $\bar{\kappa}$ . Alignment  $\text{Cov}(a, \kappa)$  is negative when accurate predictions are slow. Matching the baseline requires  $\bar{a} \geq a_0/\bar{\kappa}$  at zero alignment.

### 3.3. Amortised Utility

**Scenario.** Both preceding metrics impose per-batch temporal structure, tying deadlines or penalties to individual processing events. Some deployments instead constrain total overhead while remaining agnostic to its distribution. Edge devices, for instance, may budget computation across an overnight session. Varying this budget traces a curve characterising the accuracy-budget trade-off, addressing how much accuracy a method purchases per unit overhead.

**Protocol.** Let  $c_i = \delta_i - \lambda$  denote adaptation overhead for batch  $i$ . Given budget  $B \geq 0$ , we define the cutoff  $m = \max\{j : \sum_{i=1}^j c_i \leq B\}$ . For  $i \leq m$ , adaptation proceeds; for  $i > m$ , the model freezes at state  $\theta_m$  and inference continues without updates. This models deployments where users require results within a time envelope but don't penalise intermediate latency.

**Metric.** Let  $\beta = m/N$  denote the adapted fraction. Amortised utility is formally:

$$U_{\text{amortised}} = \beta \cdot \bar{a}_{\text{adapt}} + (1 - \beta) \cdot \bar{a}_{\text{frozen}} \quad (3)$$

where  $\bar{a}_{\text{adapt}}$  and  $\bar{a}_{\text{frozen}}$  are mean accuracies over adapted and frozen phases. The decomposition reveals whether adaptation gains persist after budget exhaustion:  $\bar{a}_{\text{frozen}} < a_0$  indicates adaptation-induced drift that harms post-freeze performance;  $\bar{a}_{\text{frozen}} > a_0$  indicates adaptation contributed durable improvements by amortising the initial overhead. Not all methods are stateful or exhaust the budget; comparison across methods occurs via Pareto efficiency over varying  $B$ , identifying which method delivers maximum value at each budget and where returns diminish.

## 4. Time-Contingent Evaluation

We evaluate seven Fully TTA methods: AdaBN (Li et al., 2017), LAME (Boudiaf et al., 2022), NEO (Murphy et al., 2025), Tent (Wang et al., 2021), ETA (Niu et al., 2022), SHOT-IM (Liang et al., 2020), and SAR (Niu et al., 2023); the first three are gradient-free, and the last four are gradient-based. Standard inference is the non-adaptive baseline.

Following Niu et al. (2022) and Alfarra et al. (2024), we evaluate on ImageNet-C (Hendrycks & Dietterich, 2019) at severity level 5, which comprises 15 corruption types across four categories (noise, blur, weather, digital) applied to the ImageNet validation set (Russakovsky et al., 2015). Evaluation is *episodic*, with methods reset between corruptions and batches sampled i.i.d. within each; all methods use their supplied default hyperparameters. We use an ImageNet-pretrained ResNet-50 (He et al., 2016) backbone with batch size 64 and evaluate on an Nvidia RTX 4080 GPU, where standard inference processes batches in  $\approx 38.67$  ms. We set  $\lambda = 39.9$  ms using a  $6\sigma$  provision, targeting five-nines availability common in production systems.

### 4.1. Evaluation Setup

We evaluate across 16 temporal scenarios spanning the three protocols of §3, each grounded in deployment realities. Relaxing temporal pressure recovers offline rankings (Table 1), establishing a continuum to unconstrained evaluation. For brevity, both this table and Figure 3 focus on four representative corruptions. Across all 15 types, this yields 240 evaluations per method; extended results appear in Appendix C.

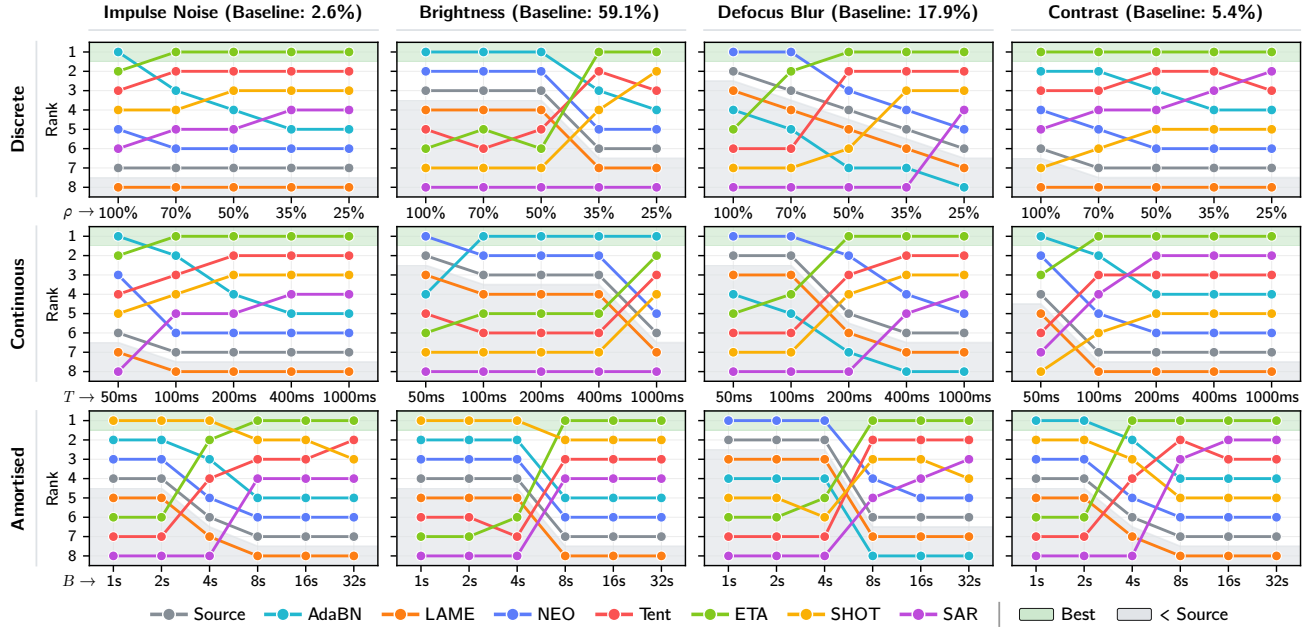


**Figure 3. Rank instability across temporal scenarios and corruption types.** Rows show discrete (utilisation  $\rho$ ), continuous (threshold  $T$ ), and amortised (budget  $B$ ) evaluations; columns show one corruption from each category, spanning baseline accuracies from 2.6% to 59.1%. Green regions mark the best method; grey regions mark methods worse than standard inference. At relaxed thresholds, rankings converge towards offline; under pressure, instability increases. No method dominates. Best viewed in colour.

**Discrete Utility.** Utilisation  $\rho = \lambda/\gamma$  controls how tightly the inter-arrival time  $\gamma$  is coupled to the baseline latency  $\lambda$ . We evaluate at  $\rho \in \{100, 70, 50, 35, 25\}\%$ , corresponding to  $\gamma \in \{39.9, 56.4, 79.8, 112.8, 159.6\}$  ms. This follows  $\sqrt{2}$  geometric spacing for uniform logarithmic coverage. These values map to practical deployment capacities. Consider, for instance, an in-store video surveillance system processing 30 fps streams with a batch size of 64. At  $\rho = 100\%$ , the saturated pipeline processes 1,604 samples per second, supporting approximately 53 cameras with no slack for adaptation; at  $\rho = 25\%$ , capacity drops to 13 cameras but provides 4× headroom. The spacing captures this trade-off between system capacity and adaptation tolerance.

**Continuous Utility.** Threshold  $T$ , which we ground in HCI research on perceived responsiveness (Nielsen, 1994; Card et al., 1983), sets the half-life for prediction value: utility halves when total response time reaches  $T$ ; adaptation overhead up to  $T - \lambda$  retains at least half the initial accuracy. We evaluate at  $T \in \{50, 100, 200, 400, 1000\}$  ms, corresponding to overhead tolerances of  $\approx \{10, 60, 160, 360, 960\}$  ms. Researchers with different  $\lambda$  can anchor  $T$  to their system’s responsiveness constraints. Consider an on-device photo organiser that auto-tags images during bulk upload: at  $T = 50$  ms, users expect instant tagging and tolerate negligible overhead; at  $T = 1000$  ms, users accept a brief pause for improved accuracy. Varying  $T$  models user or downstream expectations of system responsiveness, from latency-critical interfaces to tolerant background tasks.

**Table 1.** Offline accuracy (%) with ranks for the four corruptions in Figure 3. ETA ranks first across all 15; we show four for brevity.

Method	Corruptions			
	Impulse	Brightness	Defocus	Contrast
Standard	2.64 (7)	59.13 (7)	17.91 (6)	5.38 (7)
AdaBN	16.67 (5)	65.33 (5)	15.10 (8)	16.87 (4)
LAME	2.24 (8)	58.74 (8)	17.63 (7)	5.15 (8)
NEO	5.18 (6)	60.27 (6)	21.11 (5)	8.07 (6)
Tent	31.27 (3)	67.47 (3)	27.72 (3)	26.34 (3)
ETA	<b>38.18</b> (1)	<b>67.85</b> (1)	<b>33.19</b> (1)	<b>45.63</b> (1)
SHOT-IM	30.81 (4)	67.62 (2)	27.31 (4)	13.15 (5)
SAR	32.58 (2)	67.41 (4)	29.10 (2)	38.26 (2)

**Amortised Utility.** Budget  $B$  caps cumulative adaptation overhead; once exhausted, the model freezes for the remaining batches. With  $N = 781$  batches per corruption, processing with standard inference takes  $\lambda N \approx 31$  s. We evaluate  $B \in \{1, 2, 4, 8, 16, 32\}$  s, spanning 3% to 105% of this baseline in power-of-two increments; researchers can scale  $B$  to their deployment’s overhead tolerance. Consider a drone performing visual crop inspection that continuously captures and batches images for onboard classification; its flight time and onboard compute are battery-constrained. At  $B = 1$  s, minimal adaptation preserves resources to maximise field coverage. At  $B = 32$  s, more adaptation possibly restricts this coverage. The budget reflects resource commitment, and our evaluation reveals how much was consumed and whether it yielded gains over standard inference.

Table 2. Per-batch overhead decomposition ( $\lambda = 39.9$  ms; notation per §3), averaged across 11,715 batches. The last four methods are gradient-based. Timings vary by chosen hardware platform.

Method	Latency Breakdown (ms)			Slowdown	
	$\bar{\delta}$	$\bar{e}$	$\bar{e} - \lambda$		
Standard	38.7	38.7	0.0	0.0	0.97×
AdaBN	41.1	41.1	1.2	0.0	1.03×
LAME	40.3	40.3	0.3	0.0	1.01×
NEO	38.8	38.8	0.0	0.0	0.97×
Tent	97.1	41.1	1.2	56.1	2.43×
ETA	97.7	41.1	1.2	56.6	2.45×
SHOT-IM	121.0	41.1	1.2	79.8	3.03×
SAR	195.2	41.1	1.2	154.1	4.89×

## 4.2. Rank Instability

Figure 3 reveals that rankings are unstable across temporal scenarios and corruption types. ETA, the clear offline winner, achieves the first rank in only 141 of 240 evaluations (58.8%); upon losing, it yields 19.3% utility on average to the winner, and underperforms standard inference in 57 evaluations (23.8%). This instability exhibits a sharp transition: at high pressure ( $\rho = 100\%$ ,  $T = 50$  ms,  $B \leq 2$  s), its win rate drops to 0–7%; at low pressure, it recovers to 93–100%.

Table 2 decomposes per-batch latency to reveal the root cause: intrinsic overhead  $\bar{e} - \lambda$  from modified forward passes is negligible across all methods (0–1.2 ms), while extrinsic overhead  $\bar{\ell}$  from backpropagation dominates for gradient-based methods at 56–154 ms, yielding 2.4–4.9× slowdowns. This cost, invisible to offline evaluation, determines whether a method can keep pace with temporal pressure.

**Method Selection.** Instability varies across corruptions. Under  $T = 50$  ms, Spearman correlation with the offline ranking ranges from  $r_s = -0.74$  (brightness) to  $r_s = 0.21$  (Gaussian noise); under  $\rho = 100\%$ , from  $r_s = -0.62$  (frost) to  $r_s = 0.74$  (contrast). Per-corruption rankings do not follow a fixed pattern across scenarios; temporal pressure triggers the instability while corruption characteristics modulate its severity. As pressure relaxes, offline rankings become more predictive: under discrete evaluation, correlation rises from  $r_s = -0.04$  at  $\rho = 100\%$  to  $r_s = 0.95$  at  $\rho = 25\%$ ; under amortised evaluation, from  $r_s = 0.32$  at  $B = 4$  s to  $r_s = 0.96$  at  $B = 8$  s. While specific thresholds vary with model and dataset, practitioners should validate method selection under their deployment’s temporal constraints rather than relying on offline rankings alone.

## 4.3. Trade-Off Analysis

Utility decompositions reveal protocol-specific bottlenecks that explain why rankings are unstable. We analyse the strictest temporal scenarios for each protocol ( $\rho = 100\%$ ,  $T = 50$  ms,  $B = 1$  s), where instability is most pronounced.

Table 3. Discrete utility decomposition at  $\rho = 100\%$ , aggregated across 15 corruptions (11,715 batches). Availability  $\alpha$ , the fraction of batches served, determines ranking despite gradient-based methods achieving higher served accuracy.

Method	$\alpha$ (%)	$ \mathcal{P} $	$\bar{a}_{\text{served}}$ (%)	$U_{\text{discrete}}$ (%)
Standard	100.0	11,715	18.2	18.2
AdaBN	97.2	11,388	31.7	<b>30.8</b>
LAME	98.8	11,579	17.5	17.3
NEO	100.0	11,715	22.1	<u>22.1</u>
Tent	41.2	4,830	40.4	16.6
ETA	41.0	4,800	<b>45.6</b>	18.7
SHOT-IM	33.2	3,885	<u>40.6</u>	13.5
SAR	20.6	2,415	37.6	7.8

Decompositions shown aggregate across all 15 corruptions.

Table 3 shows discrete utility following Equation (1) at  $\rho = 100\%$ . ETA achieves the highest served accuracy (45.6%) but serves only 41% of batches; the product yields 18.7% utility. Meanwhile, AdaBN’s served accuracy is lower (31.7%) but its 97.2% availability yields 30.8% utility, a 12.1% utility gain over ETA. Availability places a ceiling on a method’s achievable utility; even at 100% served accuracy, serving  $\alpha$  fraction of batches achieves at most  $\alpha$  utility. When this ceiling falls below a competitor’s utility, no accuracy gain can compensate; we term this state *computational insolvency*. To match AdaBN, ETA would need 75.1% served accuracy, far exceeding any observed TTA performance on ImageNet-C; to do the same, SAR would need 149.5%, a mathematical impossibility.

Table 4 shows continuous utility following Equation (2) at  $T = 50$  ms. Unlike availability, responsiveness imposes a multiplicative penalty rather than a ceiling; every prediction is served, but late predictions lose value. ETA’s 48.4% accuracy is discounted by 85% to yield just 7.2% utility. AdaBN’s 90% responsiveness preserves most of its 31.7% accuracy, yielding 28.4% utility. To close this gap, ETA would require 189% accuracy, signalling insolvency by multiplication rather than exclusion; the insolvency threshold varies by corruption. On brightness at  $T = 50$  ms, where baseline accuracy is already 59.1%, standard inference outperforms all gradient-based methods; the overhead cannot be justified when return on compute is limited.

Table 5 shows amortised utility following Equation (3) at  $B = 1$  s. Per corruption, gradient-based methods exhaust their budget within the first  $\sim 20$  batches, freezing for the remaining 97%; what happens after freezing determines utility. Tent, ETA, and SAR collapse to 0.1% frozen accuracy, dragging overall utility below 1%, 20× worse than standard inference. Insolvency here takes the form of unproductive overhead: budget consumed without lasting gains. Surprisingly, SHOT-IM, despite higher per-batch overhead than ETA (79.8 ms vs 56.6 ms), maintains 32.2% frozen accu-

Table 4. Continuous utility decomposition at  $T = 50$  ms. Responsiveness  $\bar{\kappa}$  determines ranking; alignment near unity indicates accuracy and responsiveness are approximately independent.

Method	$\bar{a}$ (%)	$\bar{\kappa}$ (%)	$\text{Cov}(a, \kappa)$	$U_{\text{continuous}}$ (%)
Standard	18.16	100.0	1.000	18.16
AdaBN	31.72	89.6	1.000	<b>28.42</b>
LAME	17.40	95.7	1.018	16.96
NEO	22.14	100.0	1.000	<u>22.14</u>
Tent	42.88	15.1	0.998	6.46
ETA	<b>48.35</b>	15.0	0.998	7.22
SHOT-IM	<u>42.43</u>	11.2	0.998	4.73
SAR	44.14	6.2	0.995	2.73

racy, matching its adapted accuracy and yielding the highest utility among gradient-based methods. This resilience is invisible to offline evaluation. We speculate this stems from SHOT-IM’s information maximisation objective, which stabilises representations even when parameter updates cease.

**Method design.** These decompositions reveal three failure modes: availability collapse, accuracy erosion, and unproductive overhead; all stem from overhead not justified by accuracy gains under temporal pressure. Addressing these failures requires three properties absent from current methods. First, *corruption-conditioned allocation*: corruptions perturb features differently, yet current methods apply fixed mechanisms with uniform overhead; brightness shifts all pixels uniformly and corrects cheaply, while Gaussian noise perturbs pixels independently, requiring more compute to recover structure. Second, *time-aware scaling*: methods should bound response delay to promptly conclude adaptation before deadlines or discounting erases gains. Third, *anytime performance*: elapsed overhead should yield gains over standard inference regardless of when adaptation halts. Methods that degrade before improving, as Tent, ETA, and SAR do under amortised evaluation, risk leaving prediction worse than if adaptation had never begun. We view all three properties as essential for deployable adaptation.

## 5. Discussion

Our evaluation is scoped to the canonical TTA context of image classification on ImageNet-C with ResNet-50 to enable direct comparison with prior work. Even in this well-studied benchmark, Tempora reveals rank instability. While distinct modalities (text, audio), tasks (segmentation, translation), domains (wildlife monitoring, medical imaging), architectures (vision transformers, mobile-optimised networks), and hardware (single-board computers, microcontrollers) entail unique trade-offs, the underlying need to reconcile adaptation overhead with deployment constraints remains universal, as do the design requirements we identify in §4.3.

Within this context, we evaluate seven Fully TTA methods, balancing coverage with tractable overhead. This rules out

Table 5. Amortised utility decomposition at  $B = 1$  s. For gradient-based methods, frozen accuracy determines rankings. For gradient-free methods, adapt accuracy determines ranking.

Method	$\beta$ (%)	$\bar{a}_{\text{adapt}}$ (%)	$\bar{a}_{\text{frozen}}$ (%)	$U_{\text{amortised}}$ (%)
Standard	100.0	18.16	-	18.16
AdaBN	100.0	31.72	-	<u>31.72</u>
LAME	99.9	17.42	3.81	17.40
NEO	100.0	22.14	-	22.14
Tent	2.3	32.11	0.10	0.84
ETA	2.3	33.37	0.10	0.87
SHOT-IM	1.7	32.23	<b>32.22</b>	<b>32.22</b>
SAR	0.9	33.54	0.10	0.40

methods that perform multiple forward passes before back-propagation (Marsden et al., 2024; Lee et al., 2024; Ma et al., 2025; Niu et al., 2025); their incremental gains are unlikely to offset the additional overhead under temporal pressure. We also exclude wrapper-like methods (Zhao et al., 2023a; Zhang et al., 2025; Kim et al., 2025), which would combinatorially expand the evaluation space and are left as future work. Beyond these exclusions, our episodic, i.i.d. evaluation affects method fit: LAME (Boudiaf et al., 2022), designed for non-i.i.d. streams, underperforms standard inference in all 240 cases, illustrating that method-evaluation mismatch can render adaptation counterproductive.

Such mismatches motivate evaluating methods in contexts suited to their design. The distributional realism efforts discussed in §2 provide fairer settings for methods targeting continual, non-stationary streams (Wang et al., 2022; Yuan et al., 2023; Song et al., 2023; Hong et al., 2023). Though out of scope, integrating Tempora with such evaluations could model complex deployments and inform application-specific methods. Moreover, while we present each utility metric for a distinct scenario, they can be combined to model richer temporal dynamics; a battery-operated person detector, where visitors arrive asynchronously and notifications must be prompt, would require all three utility metrics.

## 6. Conclusion

We introduced *Tempora*, a framework for evaluating TTA methods under temporal pressure, comprising three metrics that characterise time-contingent utility under distinct deployment constraints. Each decomposes into interpretable factors revealing why methods succeed or fail. Across 240 temporal evaluations, we find rank instability is pervasive: offline rankings do not predict rankings under temporal pressure. Utility decompositions expose three failure modes stemming from overhead that accuracy gains cannot justify. Addressing these to realise deployable adaptation requires corruption-conditioned overhead allocation, time-aware scaling, and anytime performance. Tempora provides the lens to evaluate progress toward this goal.

## Impact Statement

This paper promotes more realistic evaluation of test-time adaptation by accounting for a range of latency constraints that arise in real-world deployments. By exposing how conventional rankings can fail under temporal pressure, *Tempora* helps practitioners select methods suited to application-specific time budgets and provides researchers with design targets for deployable adaptation. The proposed evaluation framework does not introduce new adaptive capabilities, but rather improves transparency around existing methods, supporting more responsible and deployment-aware use of adaptable machine learning systems.

## References

Alfarrà, M., Itani, H., Pardo, A., Alhuwaider, S. Y., Ramazanova, M., Perez, J. C., Cai, Z., Müller, M., and Ghanem, B. Evaluation of test-time adaptation under computational time constraints. In Salakhutdinov, R., Kolter, Z., Heller, K., Weller, A., Oliver, N., Scarlett, J., and Berkenkamp, F. (eds.), *Proceedings of the 41st International Conference on Machine Learning*, volume 235 of *Proceedings of Machine Learning Research*, pp. 976–991. PMLR, 21–27 Jul 2024. URL <https://proceedings.mlr.press/v235/alfarra24a.html>.

Apple. A Multi-Task Neural Architecture for On-Device Scene Analysis, 2022. URL <https://machinelearning.apple.com/research/on-device-scene-analysis>.

Bommasani, R., Hudson, D. A., Adeli, E., Altman, R., Arora, S., von Arx, S., Bernstein, M. S., Bohg, J., Bosslut, A., Brunskill, E., Brynjolfsson, E., Buch, S., Card, D., Castellon, R., Chatterji, N. S., Chen, A. S., Creel, K. A., Davis, J., Demszky, D., Donahue, C., Doumbouya, M., Durmus, E., Ermon, S., Etchemendy, J., Ethayarajh, K., Fei-Fei, L., Finn, C., Gale, T., Gillespie, L. E., Goel, K., Goodman, N. D., Grossman, S., Guha, N., Hashimoto, T., Henderson, P., Hewitt, J., Ho, D. E., Hong, J., Hsu, K., Huang, J., Icard, T. F., Jain, S., Jurafsky, D., Kalluri, P., Karamcheti, S., Keeling, G., Khani, F., Khattab, O., Koh, P. W., Krass, M. S., Krishna, R., Kuditipudi, R., Kumar, A., Ladhak, F., Lee, M., Lee, T., Leskovec, J., Levent, I., Li, X. L., Li, X., Ma, T., Malik, A., Manning, C. D., Mirchandani, S. P., Mitchell, E., Munyikwa, Z., Nair, S., Narayan, A., Narayanan, D., Newman, B., Nie, A., Niebles, J. C., Nilforoshan, H., Nyarko, J. F., Ogut, G., Orr, L., Papadimitriou, I., Park, J. S., Piech, C., Portelance, E., Potts, C., Raghunathan, A., Reich, R., Ren, H., Rong, F., Roohani, Y. H., Ruiz, C., Ryan, J., R'e, C., Sadigh, D., Sagawa, S., Santhanam, K., Shih, A., Srinivasan, K. P., Tamkin, A., Taori, R., Thomas, A. W., Tramèr, F., Wang, R. E., Wang, W., Wu, B., Wu, J., Wu, Y., Xie, S. M., Yasunaga, M., You, J., Zaharia, M. A., Zhang, M., Zhang, T., Zhang, X., Zhang, Y., Zheng, L., Zhou, K., and Liang, P. On the opportunities and risks of foundation models. *ArXiv*, 2021. URL <https://crfm.stanford.edu/assets/report.pdf>.

Boudiaf, M., Mueller, R., Ayed, I. B., and Bertinetto, L. Parameter-free Online Test-time Adaptation. In 2022 IEEE/CVF Conference on Computer Vision and Pattern Recognition (CVPR), pp. 8334–8343, New Orleans, LA, USA, June 2022. IEEE. ISBN 9781665469463. doi: 10.1109/CVPR52688.2022.00816. URL <https://ieeexplore.ieee.org/document/9879724/>.

Brocas, I., Carrillo, J. D., and Tarrasó, J. How long is a minute? *Games and Economic Behavior*, 111:305–322, 2018. ISSN 0899-8256. doi: <https://doi.org/10.1016/j.geb.2018.06.007>. URL <https://www.sciencedirect.com/science/article/pii/S089982561830112X>.

Card, S. K., Newell, A., and Moran, T. P. *The Psychology of Human-Computer Interaction*. L. Erlbaum Associates Inc., USA, 1983. ISBN 0898592437.

Danilowski, M., Chatterjee, S., and Ghosh, A. Botta: Benchmarking on-device test time adaptation, 2025. URL <https://arxiv.org/abs/2504.10149>.

Dorfner, F. J., Patel, J. B., Kalpathy-Cramer, J., Gerstner, E. R., and Bridge, C. P. A review of deep learning for brain tumor analysis in mri. *npj Precision Oncology*, 9(1), January 2025. ISSN 2397-768X. doi: 10.1038/s41698-024-00789-2. URL <http://dx.doi.org/10.1038/s41698-024-00789-2>.

Du, C., Guo, J., Wang, Y., and Huang, G. UniTTA: Unified benchmark and versatile framework towards realistic test-time adaptation. In Second Workshop on Test-Time Adaptation: Putting Updates to the Test! at ICML 2025, 2025. URL <https://openreview.net/forum?id=Qmi7gVQOTE>.

Gao, J., Zhang, J., Liu, X., Darrell, T., Shelhamer, E., and Wang, D. Back to the source: Diffusion-driven adaptation to test-time corruption. In Proceedings of the IEEE/CVF Conference on Computer Vision and Pattern Recognition (CVPR), pp. 11786–11796, June 2023.

He, K., Zhang, X., Ren, S., and Sun, J. Deep Residual Learning for Image Recognition. In 2016 IEEE Conference on Computer Vision and Pattern Recognition (CVPR), pp. 770–778, Las Vegas, NV, USA, June 2016. IEEE. ISBN 9781467388511. doi: 10.1109/CVPR.2016.90. URL <http://ieeexplore.ieee.org/document/7780459/>.

Hendrycks, D. and Dietterich, T. Benchmarking neural network robustness to common corruptions and perturbations. In *International Conference on Learning Representations*, 2019. URL <https://openreview.net/forum?id=HJz6tiCqYm>.

Hong, J., Lyu, L., Zhou, J., and Spranger, M. MECTA: Memory-economic continual test-time model adaptation. In *The Eleventh International Conference on Learning Representations*, 2023. URL <https://openreview.net/forum?id=N92hjSf5NNh>.

Kim, H., Han, G., and Hwang, D. Buffer layers for test-time adaptation. In *The Thirty-ninth Annual Conference on Neural Information Processing Systems*, 2025. URL <https://openreview.net/forum?id=sSZ9OM08KT>.

Lee, J., Jung, D., Lee, S., Park, J., Shin, J., Hwang, U., and Yoon, S. Entropy is not enough for test-time adaptation: From the perspective of disentangled factors. In *The Twelfth International Conference on Learning Representations*, 2024. URL <https://openreview.net/forum?id=9w3iw8wDuE>.

Li, Y., Wang, N., Shi, J., Liu, J., and Hou, X. Revisiting batch normalization for practical domain adaptation, 2017. URL <https://openreview.net/forum?id=BJuysoFeg>.

Liang, J., Hu, D., and Feng, J. Do we really need to access the source data? Source hypothesis transfer for unsupervised domain adaptation. In III, H. D. and Singh, A. (eds.), *Proceedings of the 37th International Conference on Machine Learning*, volume 119 of *Proceedings of Machine Learning Research*, pp. 6028–6039. PMLR, 13–18 Jul 2020. URL <https://proceedings.mlr.press/v119/liang20a.html>.

Liu, Y., Kothari, P., van Delft, B., Bellot-Gurlet, B., Mordan, T., and Alahi, A. Ttt++: When does self-supervised test-time training fail or thrive? In Ranzato, M., Beygelzimer, A., Dauphin, Y., Liang, P., and Vaughan, J. W. (eds.), *Advances in Neural Information Processing Systems*, volume 34, pp. 21808–21820. Curran Associates, Inc., 2021. URL [https://proceedings.neurips.cc/paper\\_files/paper/2021/file/b618c3210e934362ac261db280128c22-Paper.pdf](https://proceedings.neurips.cc/paper_files/paper/2021/file/b618c3210e934362ac261db280128c22-Paper.pdf).

Ma, K., Tang, J., Guo, B., Dang, F., Liu, S., Zhu, Z., Wu, L., Fang, C., Chen, Y.-C., Yu, Z., and Liu, Y. Surgeon: Memory-adaptive fully test-time adaptation via dynamic activation sparsity. In *Proceedings of the IEEE/CVF Conference on Computer Vision and Pattern Recognition (CVPR)*, pp. 30514–30523, June 2025.

Marsden, R. A., Dobler, M., and Yang, B. Universal Test-time Adaptation through Weight Ensembling, Diversity Weighting, and Prior Correction . In *2024 IEEE/CVF Winter Conference on Applications of Computer Vision (WACV)*, pp. 2543–2553, Los Alamitos, CA, USA, Jan 2024. IEEE Computer Society. doi: 10.1109/WACV57701.2024.00254. URL <https://doi.ieee.org/10.1109/WACV57701.2024.00254>.

Mazur, J. E. An adjusting procedure for studying delayed reinforcement. In Commons, M. L., Mazur, J. E., Nevin, J. A., and Rachlin, H. (eds.), *The Effect of Delay and of Intervening Events on Reinforcement Value*, pp. 55–73. Lawrence Erlbaum Associates, Hillsdale, NJ, 1987.

Murphy, A., Danilowski, M., Chatterjee, S., and Ghosh, A. Neo: No-optimization test-time adaptation through latent re-centering, 2025. URL <https://arxiv.org/abs/2510.05635>.

Nielsen, J. *Usability Engineering*. Morgan Kaufmann Publishers Inc., San Francisco, CA, USA, 1994. ISBN 9780080520292.

Niu, S., Wu, J., Zhang, Y., Chen, Y., Zheng, S., Zhao, P., and Tan, M. Efficient test-time model adaptation without forgetting. In Chaudhuri, K., Jegelka, S., Song, L., Szepesvari, C., Niu, G., and Sabato, S. (eds.), *Proceedings of the 39th International Conference on Machine Learning*, volume 162 of *Proceedings of Machine Learning Research*, pp. 16888–16905. PMLR, 17–23 Jul 2022. URL <https://proceedings.mlr.press/v162/niu22a.html>.

Niu, S., Wu, J., Zhang, Y., Wen, Z., Chen, Y., Zhao, P., and Tan, M. Towards stable test-time adaptation in dynamic wild world. In *The Eleventh International Conference on Learning Representations*, 2023. URL <https://openreview.net/forum?id=g2YraF75Tj>.

Niu, S., Chen, G., Zhao, P., Wang, T., Wu, P., and Shen, Z. Self-bootstrapping for versatile test-time adaptation. In *Forty-second International Conference on Machine Learning*, 2025. URL <https://openreview.net/forum?id=Li4rieeC1O>.

Russakovsky, O., Deng, J., Su, H., Krause, J., Satheesh, S., Ma, S., Huang, Z., Karpathy, A., Khosla, A., Bernstein, M., Berg, A. C., and Fei-Fei, L. Imagenet large scale visual recognition challenge. *International Journal of Computer Vision*, 115(3):211–252, April 2015. ISSN 1573-1405. doi: 10.1007/s11263-015-0816-y. URL <http://dx.doi.org/10.1007/s11263-015-0816-y>.

Song, J., Lee, J., Kweon, I. S., and Choi, S. Ecotta: Memory-efficient continual test-time adaptation via self-distilled

regularization. In *Proceedings of the IEEE/CVF Conference on Computer Vision and Pattern Recognition (CVPR)*, pp. 11920–11929, June 2023.

Sugiyama, M., Krauledat, M., and Müller, K.-R. Covariate shift adaptation by importance weighted cross validation. *J. Mach. Learn. Res.*, 8:985–1005, December 2007. ISSN 1532-4435.

Sun, Y., Wang, X., Liu, Z., Miller, J., Efros, A., and Hardt, M. Test-time training with self-supervision for generalization under distribution shifts. In III, H. D. and Singh, A. (eds.), *Proceedings of the 37th International Conference on Machine Learning*, volume 119 of *Proceedings of Machine Learning Research*, pp. 9229–9248. PMLR, 13–18 Jul 2020. URL <https://proceedings.mlr.press/v119/sun20b.html>.

Wang, D., Shelhamer, E., Liu, S., Olshausen, B., and Darrell, T. Tent: Fully test-time adaptation by entropy minimization. In *International Conference on Learning Representations*, 2021. URL <https://openreview.net/forum?id=uX13bZLkr3c>.

Wang, Q., Fink, O., Van Gool, L., and Dai, D. Continual test-time domain adaptation. In *Proceedings of Conference on Computer Vision and Pattern Recognition*, 2022.

Yuan, L., Xie, B., and Li, S. Robust test-time adaptation in dynamic scenarios. In *Proceedings of the IEEE/CVF Conference on Computer Vision and Pattern Recognition (CVPR)*, pp. 15922–15932, June 2023.

Zhang, Q., Bian, Y., Kong, X., Zhao, P., and Zhang, C. COME: Test-time adaption by conservatively minimizing entropy. In *The Thirteenth International Conference on Learning Representations*, 2025. URL <https://openreview.net/forum?id=506BjJ1ziZ>.

Zhao, B., Chen, C., and Xia, S.-T. DELTA: DEGRADATION-FREE FULLY TEST-TIME ADAPTATION. In *The Eleventh International Conference on Learning Representations*, 2023a. URL <https://openreview.net/forum?id=eGm22rqG93>.

Zhao, H., Liu, Y., Alahi, A., and Lin, T. On pitfalls of test-time adaptation. In Krause, A., Brunskill, E., Cho, K., Engelhardt, B., Sabato, S., and Scarlett, J. (eds.), *Proceedings of the 40th International Conference on Machine Learning*, volume 202 of *Proceedings of Machine Learning Research*, pp. 42058–42080. PMLR, 23–29 Jul 2023b. URL <https://proceedings.mlr.press/v202/zhao23d.html>.

## A. Notation & Terminology

Table 6 summarises the notation used throughout the paper. Table 7 defines key terms.

The terms “*online*” and “*offline*” are overloaded in the TTA literature. Alfarra et al. (2024) use online to denote evaluation under temporal constraints, *i.e.*, live, real-time processing, and offline to denote relaxed evaluation without such constraints. We adopt this interpretation of offline in our work. Our use of online, however, refers to sequential evaluation where the model must commit to a prediction on the current batch before observing subsequent batches; this interpretation appears in Wang et al. (2021). A third setting, which one might call “*fully offline*,” provides access to the entire target domain before any predictions are required. SHOT-IM (Liang et al., 2020) and AdaBN (Li et al., 2017) were initially developed for this setting; the generality of their adaptation mechanisms, detailed in §C.1, affords transferability to the online setting we evaluate in.

Table 6. Mathematical notation grouped by context.

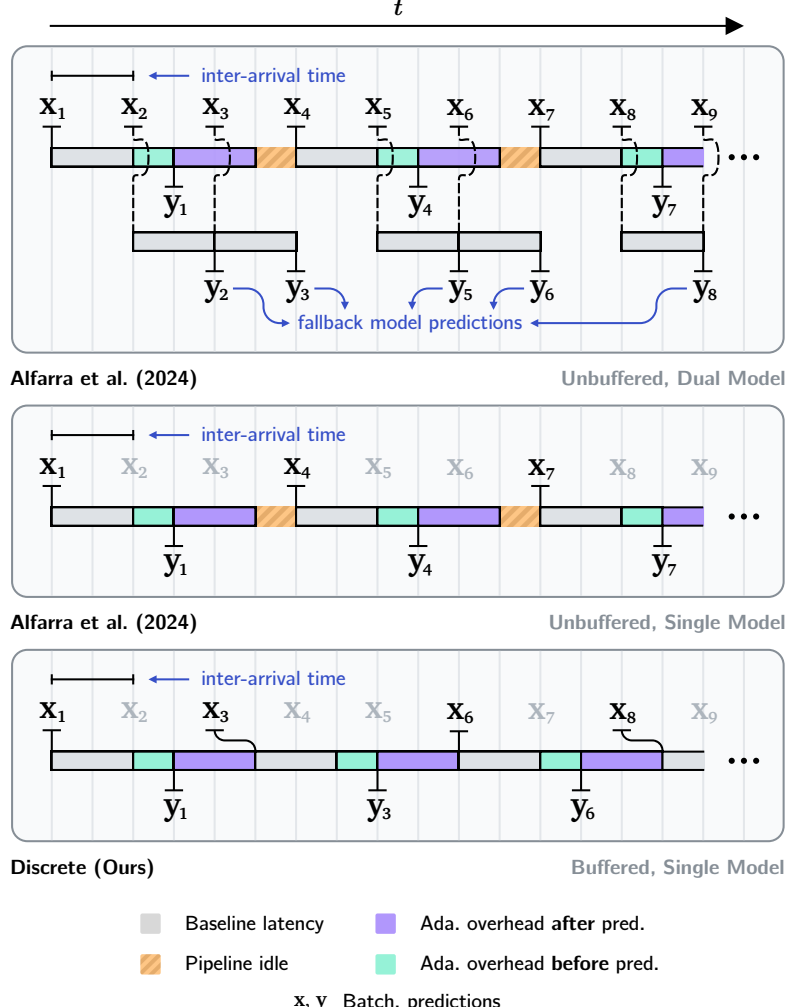
Symbol	Description	Symbol	Description
<i>General</i>			
$N$	Total number of batches	$e_i$	Intrinsic time (pickup to emission)
$\mathbf{x}_i$	Input batch $i$	$\ell_i$	Extrinsic time (emission to next pickup)
$\mathbf{y}_i$	Predictions for batch $i$	$w_i$	User wait time ( $\ell_{i-1} + e_i$ )
$t_i$	Arrival time of batch $i$	$d_i$	Effective response delay
$\delta_i$	Processing latency for batch $i$	$\kappa_i$	Decay factor (responsiveness)
$a_i$	Accuracy on batch $i$	$T$	HCI threshold
$a_0$	Standard inference accuracy	$\bar{\kappa}$	Mean responsiveness
$\lambda$	Standard inference latency	$\text{Cov}(a, \kappa)$	Accuracy-responsiveness alignment
$\theta$	Model parameters		
$r_s$	Spearman rank correlation		
<i>Discrete Utility</i>			
$\gamma$	Inter-arrival time	$c_i$	Adaptation overhead ( $\delta_i - \lambda$ )
$\rho$	Pipeline utilisation ( $\lambda/\gamma$ )	$B$	Overhead budget
$\mathcal{P}$	Set of served batch indices	$m$	Cutoff batch index (budget exhaustion)
$\alpha$	Availability ( $ \mathcal{P} /N$ )	$\beta$	Adapted fraction ( $m/N$ )
$\bar{a}_{\text{served}}(\bar{a}_s)$	Mean accuracy (served batches)	$\bar{a}_{\text{adapt}}(\bar{a}_a)$	Mean accuracy (adaptation phase)
$(s_j, f_j)$	Start/finish times of event $j$	$\bar{a}_{\text{frozen}}(\bar{a}_f)$	Mean accuracy (frozen phase)
$p_j$	Batch index served at event $j$	$\theta_m$	Frozen model state after budget exhaustion
<i>Amortised Utility</i>			

Table 7. Key terminology introduced in this paper.

Term	Definition
Fully TTA	Test-time adaptation using only pre-trained parameters $\theta$ and unlabelled target samples $x_i \sim \mathcal{T}$ , without access to source training data or supervision.
Episodic evaluation	Each corruption is treated as an independent episode, with the model and adaptation mechanism reset to its original state between corruptions.
Continual evaluation	Adaptation is cumulative across all corruptions; any updates made persists across the continuous stream. Ordering of corruptions may vary.
i.i.d. (samples)	Samples within a batch are drawn independently and identically from the target domain $\mathcal{T}$ ; no structure in class ordering or temporal dependencies.
Availability	Fraction of batches served under discrete evaluation ( $\alpha$ ); more generally, whether a model pipeline or system is ready to serve requests.
Intrinsic overhead	Added latency from a modified forward pass ( $e_i - \lambda$ ); delays the immediate response. Arises from operations such as computing batch statistics.
Extrinsic overhead	Post-prediction computation ( $\ell_i$ ); stalls the pipeline before next batch.
Responsiveness	Decay factor penalising late predictions under continuous evaluation ( $\kappa$ ).
Computational insolvency	When a method’s overhead cannot be justified by accuracy gains under temporal pressure, relative to standard inference of competing methods.
Rank instability	Phenomenon where method rankings change under temporal pressure relative to that observed in offline evaluation.
Anytime performance	Property where elapsed overhead yields gains over standard inference regardless of when adaptation halts.

## B. Discrete Protocol Design

This section expands on Tempora’s discrete protocol (§3.1) and its relationship with prior work. We compare our buffered approach with Alfarra et al.’s (2024) protocol variants (Figure 4), justify design choices, and note implementation details. Although focused on the discrete temporal setting, some observations generalise to Tempora’s broader framework.



**Figure 4. Comparison of discrete evaluation protocols.** *Top:* Alfarra et al.’s (2024) dual-model variant uses a fallback model pipeline that serves predictions for batches arriving while the primary model adapts; the dashed lines indicate these batches redirected to the second pipeline. This model may be periodically updated with the adapted state. The setup assumes zero-cost parallel model execution. *Middle:* Their single-model variant skips missed batches and forces the pipeline to idle until the next arrival. *Bottom:* Our buffered protocol retains the most recent batch, serving it when the pipeline is free. This avoids fallback assumptions and forced idling while exposing availability as the cost of slow adaptation. The legend largely remains the same as in Figure 2, with the inclusion of pipeline idling (yellow).

### B.1. Prior Work

Alfarra et al.’s (2024) protocols penalise slow adaptation with fewer batches (§2); given arrival interval  $\gamma = 40$  ms and adaptation time  $\delta_i = 75$  ms, every other batch skips adaptation. In their *dual-model* protocol, the centrepiece of their work, these “skipped” batches receive predictions from a fallback inference model, which may be periodically updated with the adapted state. This approach guarantees near-100% system availability, barring resource contention from parallel model pipelines. However, this setting imposes no constraint on the timeliness of adaptation, which operates as a secondary, passive process; adaptation affects task performance (*accuracy*), not system performance (*availability*), operating under a safety net provided by the fallback model. The primary evaluative objective then reduces to maximising accuracy as in offline evaluation, since availability is guaranteed by construction.

**Design targets.** Their focus lies in *whether* methods yield tangible returns when starved of batches under a shared, formalised penalty; ours lies in *why*, revealed through the accuracy-availability decomposition absent from their framing. When a method’s wall-clock time  $\delta_i$  fits within  $\gamma$ , the fallback only serves to add resilience. Under this framing, methods that keep pace with the stream are not distinctly rewarded beyond those that adapt periodically while skipping most batches.

We view adaptation not as an auxiliary process but as a necessary evolution of inference. [Alfarra et al.’s \(2024\)](#) framing, while valuable for benchmarking sample starvation, does not surface design targets for this transition. Tempora’s decompositions aim to provide them, facilitating deployable adaptation methods that may underlie adaptable intelligence at scale.

## B.2. Our Approach

We build on the *single-model* variant briefly noted in [Alfarra et al.’s \(2024\)](#) appendix for two reasons. First, system performance is no longer shielded from adaptation overhead: skipped batches are discarded<sup>3</sup>, which caps peak achievable utility (§4.3). Second, single-model pipelines are common in edge deployments, which host many real-world ML applications but are resource-constrained. While removing the safety net surfaces availability for discrete settings, rigid synchronisation (§2) persists, forcing the adaptation pipeline to idle on incoming batches (Figure 4).

Our view is that an evaluation protocol should remain agnostic to adaptation details where possible, presenting batches or streams with delivery constraints and letting methods decide their response. This is not to say protocols should impose no constraints; deployment realities demand some. However, these constraints should be well-motivated. Forced idling appears to be an unintended side effect of the ceiling operation in the penalty mechanism rather than a motivated constraint<sup>4</sup>. While response delay or stale adaptation could justify idling in specific deployments, these are not general evaluation concerns. We introduce a single batch-sized buffer ( $\approx 37$  MB for ImageNet) to keep the pipeline saturated.

**Buffer mechanics.** We limit the buffer to a single batch because larger buffers offer diminishing returns under fixed arrival rates; they delay the onset of evictions but do not change the steady-state eviction rate. Availability may only improve due to the drain phase, where arrivals cease with the data stream. Larger buffers are meaningful in absorbing transient surges (bursty arrivals). Modelling variable-rate streams is a derivative temporal scenario that we leave to future work.

Buffers introduce a queuing delay. Without one, batches are served immediately upon arrival. With a buffer of  $b$  batches, a batch waits at most  $b \cdot \gamma$  before being evicted or picked up for processing. The buffer size thus governs a trade-off: larger buffers absorb backlog and reduce evictions but increase response latency and data staleness. For our single batch-sized buffer, the maximum queuing delay is  $\gamma$ . Sizing beyond the utilisation factor ( $b > \rho$ ) is wasteful as the buffer never saturates.

## B.3. Implementation Details

Although both ours and [Alfarra et al.’s \(2024\)](#) discrete protocols describe asynchronous batch arrivals, the implementation operates in retrospect. In each simulation timestep where adaptation occurs, the wall-clock time  $\delta_i$  is used with the arrival interval  $\gamma$  to determine which incoming batches would be skipped; it captures adaptation overhead and its interaction with a stream without a real-time testbed.

**Timing methodology.** [Alfarra et al. \(2024\)](#) measure the arrival interval per batch by running standard inference on each input immediately before the adaptation method. While intended to account for hardware variability, this unrealistically couples the arrival rate to per-batch measurement noise and introduces potential priming effects from back-to-back model execution. We instead fix the arrival interval. As mentioned in §4, we use a  $6\sigma$  provision to account for variance in the measured standard inference latency  $\lambda$ . The measurement occurs under a full offline evaluation, including five batches of warmup and uniform batch sizes throughout<sup>5</sup>. The arrival interval  $\gamma$  is then set based on a utilisation factor  $\rho$  that controls how saturated the pipeline is:  $\gamma = \lambda/\rho$ ; this factor controls the available headroom for adaptation by intentionally idling the pipeline relative to standard inference. We vary  $\rho$  systematically for our evaluation as detailed in §4.1.

**Batch normalisation states.** A subtle implementation detail affects frozen model behaviour. In PyTorch, batch normalisation (BN) layers operate in four modes; only one uses the running buffers to normalise the incoming batch, requiring the layer to

<sup>3</sup>[Alfarra et al. \(2024\)](#) assign random predictions to these skipped batches. This lower bounds accuracy to that of a blind classifier, which is 0.1% for ImageNet-1K and 10% for CIFAR-10. For many tasks, this approach may introduce an unacceptable level of operational risk due to potential false positives. In our protocol, we submit null predictions in such cases.

<sup>4</sup>As [Alfarra et al.’s \(2024\)](#) evaluation analysis does not report availability, this subtlety may not have been apparent

<sup>5</sup>We drop the last odd-sized batch; 16 samples for ImageNet-C corruptions ( $50,000/64 = 781.25$ )

be in evaluation mode and running buffers to exist. This mode canonically applies to frozen model inference. However, many TTA implementations clear the running buffers at setup, forcing the layers to recompute normalisation statistics on each batch even after the model is nominally frozen. This introduces overhead that unintentionally persists beyond adaptation. We provide a toggle to restore the intended frozen behaviour under amortised evaluation. For methods that modify BN layers, we track running statistics over the target domain to ensure valid buffers exist for frozen inference.

## C. Extended Time-Contingent Evaluation

This section expands on §4 with method descriptions, offline baselines, corruption-aggregated sweeps across all temporal scenarios, and per-corruption analysis; the latter includes a winner table across all 240 evaluations and utility decomposition under strict pressure. We report results for a single seed; complete per-batch logs are available in the supplementary code repository. In tables reporting results, **bold** indicates best performance and underline indicates second best.

### C.1. Method Overview

We evaluate seven Fully TTA methods spanning two families (gradient-free and gradient-based), with standard inference serving as a non-adaptive baseline. This section summarises each method’s mechanism. Their hyperparameters follow original implementations and are specified in the supplementary code. Table 8 reports offline accuracy across all corruptions.

AdaBN (Li et al., 2017) recomputes normalisation statistics on the incoming batch and accumulates an exponential moving average of these statistics across batches. LAME (Boudiaf et al., 2022) only refines output probabilities via Laplacian-regularised optimisation; it constructs a  $k$ -nearest-neighbour affinity matrix in the feature space and iteratively adjusts class probabilities to balance closeness to the model’s initial beliefs with consistency among neighbours. NEO (Murphy et al., 2025) maintains a running mean of penultimate-layer features and centres each batch by subtracting this mean before classification, correcting for feature-space drift.

Tent (Wang et al., 2021), which introduced the Fully TTA paradigm, minimises the entropy of predictions by updating affine BN parameters. ETA (Niu et al., 2022) extends Tent with two-stage sample filtering: a *reliability* filter excludes high-entropy samples that produce noisy gradients and a *redundancy* filter excludes samples whose softmax probabilities are similar to a moving mean of previously adapted samples’ probabilities, avoiding repeated gradient signals. While only filtered samples inform updates, PyTorch backpropagates through the index mask and computes gradients for all samples regardless; this explains why ETA’s latency does not improve despite filtering. SHOT-IM (Liang et al., 2020) minimises entropy while maximising prediction diversity to prevent class collapse; it updates the entire feature extractor. SAR (Niu et al., 2023) uses sharpness-aware minimisation on entropy for stability; it first perturbs weights in the direction of the entropy gradient and computes an update at the perturbed point, which encourages convergence to flatter minima. Like ETA, SAR also filters high-entropy samples. It also resets the model when the moving mean of batch entropy dips below a pre-defined threshold.

Table 8. Offline accuracy (%) across all 15 ImageNet-C corruptions.

Corruption	Gradient-Free				Gradient-Based			
	Standard	AdaBN	LAME	NEO	Tent	ETA	SHOT-IM	SAR
Gaussian noise	3.00	16.15	2.58	5.23	29.98	<b>36.01</b>	29.39	<u>31.46</u>
Shot noise	3.70	16.76	3.20	6.13	31.68	<b>38.69</b>	<u>32.00</u>	31.40
Impulse noise	2.64	16.67	2.24	5.18	31.27	<b>38.18</b>	30.81	<u>32.58</u>
Defocus blur	17.91	15.10	17.63	21.11	27.72	<b>33.19</b>	27.31	<u>29.10</u>
Glass blur	9.73	15.44	8.94	12.60	26.86	<b>33.19</b>	26.77	<u>28.21</u>
Motion blur	14.71	26.22	13.89	17.76	41.14	<b>47.78</b>	<u>43.20</u>	41.70
Zoom blur	22.46	38.90	21.87	26.57	49.26	<b>52.74</b>	<u>50.44</u>	49.23
Snow	16.60	34.18	15.23	21.72	47.21	<b>52.09</b>	<u>49.11</u>	47.23
Frost	23.06	33.11	22.30	27.67	41.15	<b>45.99</b>	41.49	<u>42.47</u>
Fog	24.01	47.83	22.23	30.57	57.56	<b>60.03</b>	<u>57.84</u>	57.64
Brightness	59.13	65.33	58.74	60.27	67.47	<b>67.85</b>	<u>67.62</u>	67.41
Contrast	5.38	16.87	5.15	8.07	26.34	<b>45.63</b>	13.15	<u>38.26</u>
Elastic transform	16.51	44.18	14.60	24.93	54.63	<b>57.74</b>	<u>55.39</u>	54.65
Pixelate	20.87	49.10	20.30	26.05	58.46	<b>60.93</b>	<u>59.08</u>	58.37
JPEG compression	32.64	39.99	32.12	38.26	52.47	<b>55.22</b>	<u>52.90</u>	52.46
<b>Mean</b>	18.16	31.72	17.40	22.14	42.88	<b>48.35</b>	42.43	<u>44.14</u>

## C.2. Corruption-Aggregated Parameter Sweeps

Tables 9–11 report utility across all parameter values for each protocol, aggregated across 15 corruptions. We omit standard deviation because it would reflect corruption difficulty rather than method consistency; the former varies widely, and corruption-level breakdowns appear in the following section. Latency variance is also minimal: across 11,715 batches, standard deviations are  $<1$  ms for gradient-free methods and  $<4$  ms for gradient-based methods, negligible relative to the 50–150 ms mean differences between method families.

Table 12 summarises the temporal decomposition terms that explain utility under strict pressure. These terms are timing-derived and nearly constant across corruptions, with LAME being the exception due to its iterative optimisation converging at variable rates ( $\alpha$ : 96.9–100.0%,  $\bar{\kappa}$ : 89.6–99.8%). Under amortised evaluation at  $B = 1$  s, gradient-based methods exhaust their budget within the first 7–18 batches of 781 total ( $<3\%$  of the stream); the rest are served by frozen inference, explaining why frozen accuracy dominates overall utility.

Table 9. Discrete utility (%) across utilisation levels ( $\rho$ ), aggregated across 15 corruptions.

Method	$\rho = 100\%$	$\rho = 70\%$	$\rho = 50\%$	$\rho = 35\%$	$\rho = 25\%$
Standard	18.16	18.16	18.16	18.16	18.16
AdaBN	<b>30.83</b>	<b>31.72</b>	31.72	31.72	31.72
LAME	17.29	17.40	17.40	17.40	17.40
NEO	<u>22.14</u>	22.14	22.14	22.14	22.14
Tent	16.63	23.98	<u>34.92</u>	<u>42.88</u>	<u>42.88</u>
ETA	18.70	<u>27.25</u>	<b>39.19</b>	<b>48.35</b>	<b>48.35</b>
SHOT-IM	13.47	<u>19.24</u>	27.71	39.72	42.43
SAR	7.75	11.32	16.62	24.23	35.48

Table 10. Continuous utility (%) across HCI thresholds ( $T$ ), aggregated across 15 corruptions.

Method	$T = 50\text{ms}$	$T = 100\text{ms}$	$T = 200\text{ms}$	$T = 400\text{ms}$	$T = 1000\text{ms}$
Standard	18.16	18.16	18.16	18.16	18.16
AdaBN	<b>28.42</b>	<b>31.11</b>	<u>31.49</u>	<u>31.62</u>	31.68
LAME	16.96	17.32	17.37	17.39	17.40
NEO	<u>22.14</u>	22.14	22.14	22.14	22.14
Tent	6.46	21.98	31.60	37.00	<u>40.47</u>
ETA	7.22	<u>24.66</u>	<b>35.53</b>	<b>41.67</b>	<b>45.61</b>
SHOT-IM	4.73	18.09	28.18	34.64	39.13
SAR	2.73	12.35	22.43	30.86	38.00

Table 11. Amortised utility (%) across overhead budgets ( $B$ ), aggregated across 15 corruptions.

Method	$B = 1\text{s}$	$B = 2\text{s}$	$B = 4\text{s}$	$B = 8\text{s}$	$B = 16\text{s}$	$B = 32\text{s}$
Standard	18.16	18.16	18.16	18.16	18.16	18.16
AdaBN	<u>31.72</u>	<u>31.72</u>	31.72	31.72	31.72	31.72
LAME	17.40	17.40	17.40	17.40	17.40	17.40
NEO	22.14	22.14	22.14	22.14	22.14	22.14
Tent	0.84	1.56	24.05	<u>40.60</u>	<u>42.55</u>	<u>43.12</u>
ETA	0.87	1.68	<u>29.23</u>	<b>46.85</b>	<b>48.30</b>	<b>48.56</b>
SHOT-IM	<b>32.22</b>	<b>35.26</b>	<b>37.24</b>	40.52	42.07	42.75
SAR	0.40	0.63	1.31	36.56	39.47	42.33

Table 12. Temporal decomposition terms under strict pressure ( $\rho=100\%$ ,  $T=50\text{ms}$ ,  $B=1\text{s}$ ), aggregated across 15 corruptions.

Factor	Gradient-Free				Gradient-Based			
	Standard	AdaBN	LAME	NEO	Tent	ETA	SHOT-IM	SAR
$\alpha$ (%) at $\rho=100\%$	100.0	97.2	98.8	100.0	41.2	41.0	33.2	20.6
$\bar{\kappa}$ (%) at $T=50\text{ ms}$	100.0	89.6	95.7	100.0	15.1	15.0	11.2	6.2
$m$ at $B=1\text{s}$	–	–	–	–	18	18	13	7

### C.3. Per-Corruption Analysis

Table 13 reports the winning method for each corruption under all 16 temporal scenarios. ETA wins in 141 of 240 cases (58.8%), but its dominance is confined to relaxed settings; it seldom wins at  $\rho \geq 70\%$ ,  $T \leq 100$  ms, or  $B \leq 4$  s. AdaBN and NEO capture most high-pressure scenarios, with SHOT-IM winning under tight amortised budgets due to its frozen accuracy robustness. The phase transition from gradient-free to gradient-based winners is visible across all three protocols.

Table 13. Winning method per corruption across 240 scenarios; win counts in legend.

Corruption	Discrete ( $\rho$ %)					Continuous ( $T$ ms)					Amortised ( $B$ s)					
	100	70	50	35	25	50	100	200	400	1k	1	2	4	8	16	32
Gaussian noise	A	E	E	E	E	A	E	E	E	E	S	S	S	E	E	E
Shot noise	A	E	E	E	E	A	E	E	E	E	S	S	S	E	E	E
Impulse noise	A	E	E	E	E	A	E	E	E	E	S	S	S	E	E	E
Defocus blur	N	N	E	E	E	N	N	E	E	E	N	N	N	E	E	E
Glass blur	A	E	E	E	E	A	E	E	E	E	A	S	S	E	E	E
Motion blur	A	E	E	E	E	A	A	E	E	E	S	S	S	E	E	E
Zoom blur	A	A	E	E	E	A	A	E	E	E	A	S	S	E	E	E
Snow	A	A	E	E	E	A	A	E	E	E	S	S	S	E	E	E
Frost	A	A	E	E	E	A	A	E	E	E	S	S	S	E	E	E
Fog	A	A	E	E	E	A	A	A	E	E	A	S	S	E	E	E
Brightness	A	A	A	E	E	N	A	A	A	A	S	S	S	E	E	E
Contrast	E	E	E	E	E	A	E	E	E	E	A	A	E	E	E	E
Elastic transform	A	A	E	E	E	A	A	A	E	E	A	S	S	E	E	E
Pixelate	A	A	E	E	E	A	A	A	E	E	S	S	S	E	E	E
JPEG compression	A	A	E	E	E	N	A	E	E	E	S	S	S	E	E	E

A daBN (55)    E TA (141)    N EO (9)    S HOT-IM (35)

Tables 14–19 decompose utility under strict temporal pressure ( $\rho=100\%$ ,  $T=50$  ms,  $B=1$  s); relaxed scenarios interpolate toward offline performance and are less informative. The temporal decomposition terms ( $\alpha, \bar{\kappa}, m$ ) appear in Table 12; these are timing-derived and nearly constant across corruptions, so the per-corruption tables report only accuracy and utility. For gradient-free methods, the decomposition is near-trivial: minimal overhead yields  $\bar{a} \approx U$ . For gradient-based methods, overhead dominates: ETA achieves 36% accuracy but only 5.4% utility at  $T=50$  ms. Under amortised evaluation, Tent, ETA, and SAR show  $\bar{a}_{\text{frozen}} \approx 0.1\%$ , while SHOT-IM maintains  $\bar{a}_{\text{frozen}} \approx 18\text{--}66\%$ . SHOT-IM updates the full backbone; the others update only BN parameters, which may not yield stable frozen representations after only 7–18 batches of adaptation.

Table 14. Discrete utility (%) decomposition at  $\rho=100\%$  (gradient-free).

Corruption	Standard		AdaBN		LAME		NEO	
	$\bar{a}_s$	$U_d$	$\bar{a}_s$	$U_d$	$\bar{a}_s$	$U_d$	$\bar{a}_s$	$U_d$
Gaussian noise	3.0	3.0	16.1	15.7	2.6	2.5	5.2	5.2
Shot noise	3.7	3.7	16.7	16.3	3.2	3.1	6.1	6.1
Impulse noise	2.6	2.6	16.7	16.2	2.2	2.2	5.2	5.2
Defocus blur	17.9	17.9	15.1	14.7	17.6	17.6	21.1	21.1
Glass blur	9.7	9.7	15.4	15.0	9.0	8.9	12.6	12.6
Motion blur	14.7	14.7	26.2	25.5	13.9	13.5	17.8	17.8
Zoom blur	22.5	22.5	38.9	37.8	21.9	21.9	26.6	26.6
Snow	16.6	16.6	34.2	33.2	15.2	15.1	21.7	21.7
Frost	23.1	23.1	33.1	32.2	22.3	22.0	27.7	27.7
Fog	24.0	24.0	47.9	46.5	22.2	22.0	30.6	30.6
Brightness	59.1	59.1	65.3	63.5	58.7	58.7	60.3	60.3
Contrast	5.4	5.4	16.9	16.4	5.1	5.1	8.1	8.1
Elastic transform	16.5	16.5	44.1	42.9	14.6	14.5	24.9	24.9
Pixelate	20.9	20.9	49.1	47.7	20.3	20.1	26.0	26.0
JPEG compression	32.6	32.6	40.0	38.9	32.1	32.1	38.3	38.3

Table 15. Discrete utility (%) decomposition at  $\rho=100\%$  (gradient-based).

Corruption	Tent		ETA		SHOT-IM		SAR	
	$\bar{a}_s$	$U_d$	$\bar{a}_s$	$U_d$	$\bar{a}_s$	$U_d$	$\bar{a}_s$	$U_d$
Gaussian noise	25.9	10.7	33.1	13.5	26.9	8.9	22.5	4.6
Shot noise	27.7	11.4	35.2	14.4	29.1	9.6	24.9	5.1
Impulse noise	27.0	11.1	33.6	13.8	27.6	9.2	23.1	4.8
Defocus blur	24.0	9.9	29.8	12.2	24.7	8.2	21.5	4.4
Glass blur	23.3	9.6	29.4	12.1	23.8	7.9	21.1	4.3
Motion blur	37.0	15.3	43.9	18.0	39.2	13.0	32.7	6.7
Zoom blur	47.4	19.6	50.8	20.8	48.9	16.2	44.4	9.1
Snow	44.0	18.1	48.6	19.9	46.7	15.5	40.2	8.3
Frost	39.4	16.3	44.2	18.1	40.1	13.3	36.8	7.6
Fog	55.7	23.0	58.5	24.0	56.8	18.9	52.6	10.8
Brightness	67.5	27.8	67.7	27.8	67.4	22.3	66.8	13.8
Contrast	26.5	10.9	41.4	17.0	16.2	5.4	27.8	5.7
Elastic transform	52.6	21.7	55.8	22.9	53.4	17.7	48.3	10.0
Pixelate	57.1	23.6	59.4	24.3	57.0	18.9	54.3	11.2
JPEG compression	50.2	20.7	53.2	21.8	51.3	17.0	47.1	9.7

 Table 16. Continuous utility (%) decomposition at  $T=50$  ms (gradient-free).

Corruption	Standard		AdaBN		LAME		NEO	
	$\bar{a}$	$U_c$	$\bar{a}$	$U_c$	$\bar{a}$	$U_c$	$\bar{a}$	$U_c$
Gaussian noise	3.0	3.0	16.2	14.5	2.6	2.3	5.2	5.2
Shot noise	3.7	3.7	16.8	15.0	3.2	2.9	6.1	6.1
Impulse noise	2.6	2.6	16.7	15.0	2.2	2.0	5.2	5.2
Defocus blur	17.9	17.9	15.1	13.5	17.6	17.6	21.1	21.1
Glass blur	9.7	9.7	15.4	13.8	8.9	8.6	12.6	12.6
Motion blur	14.7	14.7	26.2	23.5	13.9	12.7	17.8	17.8
Zoom blur	22.5	22.5	38.9	34.8	21.9	21.7	26.6	26.6
Snow	16.6	16.6	34.2	30.6	15.2	14.7	21.7	21.7
Frost	23.1	23.1	33.1	29.7	22.3	21.2	27.7	27.7
Fog	24.0	24.0	47.8	42.9	22.2	21.4	30.6	30.6
Brightness	59.1	59.1	65.3	58.5	58.7	58.6	60.3	60.3
Contrast	5.4	5.4	16.9	15.1	5.1	5.1	8.1	8.1
Elastic transform	16.5	16.5	44.2	39.5	14.6	14.2	24.9	24.9
Pixelate	20.9	20.9	49.1	44.0	20.3	19.5	26.0	26.0
JPEG compression	32.6	32.6	40.0	35.8	32.1	32.0	38.3	38.3

 Table 17. Continuous utility (%) decomposition at  $T=50$  ms (gradient-based).

Corruption	Tent		ETA		SHOT-IM		SAR	
	$\bar{a}$	$U_c$	$\bar{a}$	$U_c$	$\bar{a}$	$U_c$	$\bar{a}$	$U_c$
Gaussian noise	30.0	4.5	36.0	5.4	29.4	3.3	31.5	1.9
Shot noise	31.7	4.8	38.7	5.8	32.0	3.6	31.4	1.9
Impulse noise	31.3	4.7	38.2	5.7	30.8	3.4	32.6	2.0
Defocus blur	27.7	4.2	33.2	5.0	27.3	3.0	29.1	1.8
Glass blur	26.9	4.0	33.2	4.9	26.8	3.0	28.2	1.7
Motion blur	41.1	6.2	47.8	7.1	43.2	4.8	41.7	2.6
Zoom blur	49.3	7.4	52.7	7.9	50.4	5.6	49.2	3.1
Snow	47.2	7.1	52.1	7.8	49.1	5.5	47.2	2.9
Frost	41.2	6.2	46.0	6.9	41.5	4.6	42.5	2.6
Fog	57.6	8.7	60.0	9.0	57.8	6.5	57.6	3.6
Brightness	67.5	10.2	67.8	10.2	67.6	7.6	67.4	4.2
Contrast	26.3	4.0	45.6	6.8	13.2	1.5	38.3	2.4
Elastic transform	54.6	8.2	57.7	8.6	55.4	6.2	54.6	3.4
Pixelate	58.5	8.8	60.9	9.1	59.1	6.6	58.4	3.6
JPEG compression	52.5	7.9	55.2	8.3	52.9	5.9	52.5	3.3

Table 18. Amortised utility (%) decomposition at  $B=1$  s (gradient-free).

<b>Corruption</b>	<b>Standard</b>			<b>AdaBN</b>			<b>LAME</b>			<b>NEO</b>		
	$\bar{a}_a$	$\bar{a}_f$	$U_a$	$\bar{a}_a$	$\bar{a}_f$	$U_a$	$\bar{a}_a$	$\bar{a}_f$	$U_a$	$\bar{a}_a$	$\bar{a}_f$	$U_a$
Gaussian noise	3.0	—	3.0	16.2	—	16.2	2.6	—	2.6	5.2	—	5.2
Shot noise	3.7	—	3.7	16.8	—	16.8	3.2	—	3.2	6.1	—	6.1
Impulse noise	2.6	—	2.6	16.7	—	16.7	2.2	—	2.2	5.2	—	5.2
Defocus blur	17.9	—	17.9	15.1	—	15.1	17.6	—	17.6	21.1	—	21.1
Glass blur	9.7	—	9.7	15.4	—	15.4	8.9	—	8.9	12.6	—	12.6
Motion blur	14.7	—	14.7	26.2	—	26.2	13.9	—	13.9	17.8	—	17.8
Zoom blur	22.5	—	22.5	38.9	—	38.9	21.9	—	21.9	26.6	—	26.6
Snow	16.6	—	16.6	34.2	—	34.2	15.2	—	15.2	21.7	—	21.7
Frost	23.1	—	23.1	33.1	—	33.1	22.3	—	22.3	27.7	—	27.7
Fog	24.0	—	24.0	47.8	—	47.8	22.2	—	22.2	30.6	—	30.6
Brightness	59.1	—	59.1	65.3	—	65.3	58.7	—	58.7	60.3	—	60.3
Contrast	5.4	—	5.4	16.9	—	16.9	5.1	—	5.1	8.1	—	8.1
Elastic transform	16.5	—	16.5	44.2	—	44.2	14.6	—	14.6	24.9	—	24.9
Pixelate	20.9	—	20.9	49.1	—	49.1	20.3	—	20.3	26.0	—	26.0
JPEG compression	32.6	—	32.6	40.0	—	40.0	32.1	—	32.1	38.3	—	38.3

Gradient-free methods never exhaust the budget;  $\bar{a}_f$  is undefined and utility follows offline rankings.

 Table 19. Amortised utility (%) decomposition at  $B=1$  s (gradient-based).

<b>Corruption</b>	<b>Tent</b>			<b>ETA</b>			<b>SHOT-IM</b>			<b>SAR</b>		
	$\bar{a}_a$	$\bar{a}_f$	$U_a$	$\bar{a}_a$	$\bar{a}_f$	$U_a$	$\bar{a}_a$	$\bar{a}_f$	$U_a$	$\bar{a}_a$	$\bar{a}_f$	$U_a$
Gaussian noise	18.6	0.1	0.5	19.7	0.1	0.6	19.4	18.3	18.3	18.3	0.1	0.3
Shot noise	18.3	0.1	0.5	20.3	0.1	0.6	19.0	18.6	18.6	18.3	0.1	0.3
Impulse noise	17.0	0.1	0.5	18.9	0.1	0.5	16.7	19.9	19.8	18.1	0.1	0.3
Defocus blur	15.5	0.1	0.5	16.8	0.1	0.5	13.1	11.4	11.4	16.1	0.1	0.2
Glass blur	15.4	0.1	0.5	16.5	0.1	0.5	16.1	15.1	15.2	16.5	0.1	0.2
Motion blur	26.6	0.1	0.7	27.3	0.1	0.7	26.3	27.9	27.9	27.7	0.1	0.3
Zoom blur	38.3	0.1	1.0	39.8	0.1	1.0	39.4	38.0	38.0	40.4	0.1	0.5
Snow	34.9	0.1	0.9	36.5	0.1	0.9	36.8	34.9	34.9	39.5	0.1	0.5
Frost	34.6	0.1	0.9	35.7	0.1	0.9	34.7	35.0	35.0	34.6	0.1	0.4
Fog	46.9	0.1	1.2	48.3	0.1	1.2	46.6	44.9	44.9	46.7	0.1	0.5
Brightness	64.9	0.1	1.6	64.8	0.1	1.6	64.5	65.7	65.7	67.4	0.1	0.7
Contrast	16.8	0.1	0.5	18.8	0.1	0.5	17.4	13.6	13.7	18.3	0.1	0.3
Elastic transform	41.9	0.1	1.1	43.3	0.1	1.1	42.4	43.4	43.4	44.0	0.1	0.5
Pixelate	49.4	0.1	1.2	50.0	0.1	1.2	49.5	50.7	50.7	53.6	0.1	0.6
JPEG compression	42.5	0.1	1.1	43.8	0.1	1.1	41.3	45.8	45.7	43.8	0.1	0.5

Methods exhaust budget within 7–18 batches of 781; >97% of the stream runs on frozen inference.